Analysis of Differential Efficacy and Affinity of GABA_A (α1/α2) Selective Modulators

Qurrat U. Ain,[†] Robert M. Owen,[‡] Kiyoyuki Omoto,[‡] Rubben Torella,[‡] Krishna C. Bulusu,[†] David C. Pryde,[‡] Robert C. Glen,[†] Julian E. Fuchs,*,[†,§,∥] and Andreas Bender*,[†]

[†]Centre for Molecular Informatics, Department of Chemistry, University of Cambridge, Lensfield Road, Cambridge, CB2 1EW, United Kingdom

[‡]Worldwide Medicinal Chemistry, Pfizer NPRU, The Portway Building, Granta Park, Great Abington, Cambridge, CB21 6GS, United Kingdom

[§]Institute of General, Inorganic and Theoretical Chemistry, University of Innsbruck, Innrain 82, 6020 Innsbruck, Austria

Ⓢ Supporting Information

ABSTRACT: Selective modulators of the γ-amino butyric acid (GABA_A) family of receptors have the potential to treat a range of disease states related to cognition, pain, and anxiety. While the development of various α subunit-selective modulators is currently underway for the treatment of anxiety disorders, a mechanistic understanding of the correlation between their bioactivity and efficacy, based on ligand–target interactions, is currently still lacking. In order to alleviate this situation, in the current study we have analyzed, using ligand- and structure-based methods, a data set of 5440 GABA_A modulators. The Spearman correlation (ρ) between binding activity and efficacy of compounds was calculated to be 0.008 and 0.31 against the α1 and α2 subunits of GABA receptor, respectively; in other words, the compounds had little diversity in structure and bioactivity, but they differed significantly in efficacy. Two compounds were selected as a case study for detailed interaction analysis due to the small difference in their structures and affinities ($\Delta pK_{i(comp1\_\alpha1 - comp2\_\alpha1)}$ = 0.45 log units, $\Delta pK_{i(comp1\_\alpha2 - comp2\_\alpha2)}$ = 0 log units) as compared to larger relative efficacies ($\Delta RE_{(comp1\_\alpha1 - comp2\_\alpha1)}$ = 1.03, $\Delta RE_{(comp1\_\alpha2 - comp2\_\alpha2)}$ = 0.21). Docking analysis suggested that His-101 is involved in a characteristic interaction of the α1 receptor with both compounds **1** and **2**. Residues such as Phe-77, Thr-142, Asn-60, and Arg-144 of the γ chain of the α1γ2 complex also showed interactions with heterocyclic rings of both compounds **1** and **2**, but these interactions were disturbed in the case of α2γ2 complex docking results. Binding pocket stability analysis based on molecular dynamics identified three substitutions in the loop C region of the α2 subunit, namely, G200E, I201T, and V202I, causing a reduction in the flexibility of α2 compared to α1. These amino acids in α2, as compared to α1, were also observed to decrease the vibrational and dihedral entropy and to increase the hydrogen bond content in α2 in the apo state. However, freezing of both α1 and α2 was observed in the ligand-bound state, with an increased number of internal hydrogen bonds and increased entropy. Therefore, we hypothesize that the amino acid differences in the loop C region of α2 are responsible for conformational changes in the protein structure compared to α1, as well as for the binding modes of compounds and hence their functional signaling.

KEYWORDS: benzodiazepines, GABA_A α1, GABA_A α2, relative efficacy, affinity modeling, proteochemometric modeling, selective modulators
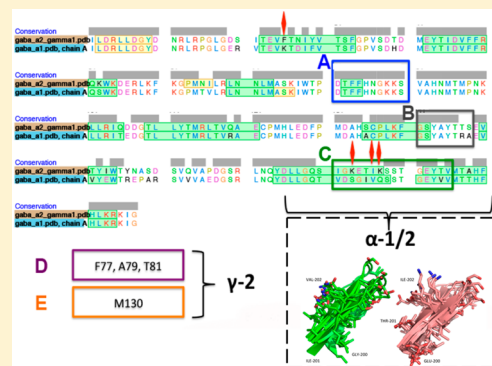
INTRODUCTION

The neurotransmitter γ-amino butyric acid (GABA) and GABA_A receptor play a key role in a wide range of important processes within the central nervous system (CNS). For example, GABA-mediated signaling is involved in cognition, learning, and pain processes, as well as disorders such as schizophrenia, anxiety, and epilepsy.[1−3] The GABA_A receptor belongs to the Cys-loop family of ligand-gated ion channels (LGIC) and modulates the flow of chloride anions across the cell membrane at the synaptic junction (as well as exterior to a synapse)[4] in response to the binding of GABA. Structurally, the GABA receptors exist as heteropentameric units, consisting mainly of two α, two β, and one γ subunits,[5] although other subunits also exist.[6,7] Multiple distinct binding sites on the receptor have been characterized, including the site for the endogenous agonist GABA, as well as naturally occurring and synthetic modulators such as neurosteroids,[8] barbiturates, and benzodiazepines.

This latter class of drugs, which was developed prior to our current understanding of GABA$_A$ pharmacology, exhibits beneficial clinical effects, but it is also associated with undesirable side effects including sedation, tolerance, dependence, and cognitive impairment. Benzodiazepines bind at the α/γ interface of the GABA receptor, act as nonselective positive allosteric modulators (PAMs) of GABA$_A$, and exert an effect at receptors containing the $\alpha 1$, $\alpha 2$, $\alpha 3$, and $\alpha 5$ subunits.[9] Subsequent genetic studies have broadly characterized the $\alpha 1$ subunit as "sedation-related", the $\alpha 2$ and $\alpha 3$ subunits as "anxiolytic-related", and the $\alpha 5$ subunit as "cognition-related" moieties.[10−12]

Building upon the positive clinical effects of benzodiazepines and this genetic evidence, researchers have explored methods to generate compounds that function as selective GABA receptor PAMs for the treatment of a wide range of CNS disorders.[13−18] For example, Merck explored the development of $\alpha 1$-sparing $\alpha 2/3$ PAMs for the treatment of anxiety.[12] During the course of these studies, it proved difficult to identify compounds that exhibited binding selectivity for the $\alpha 2/3$ receptors due to the high sequence similarity at the benzodiazepine binding site across the various α subunits. Instead, the researchers successfully identified compounds that were functionally selective for the desired population of GABA receptors. Unfortunately, our understanding of why certain ligands are functionally selective while other closely related ligands are not still remains unclear.

In order to understand the differential functional activity profile of GABA receptor modulators, we describe herein a combined ligand- and structure-based analysis of affinity and efficacy of a large number of known GABA$_A$ modulators. On the basis of compiled bioactivity data from both public and internal data sources, we employed descriptor- and receptor-based modeling approaches, including binding-mode analysis and molecular dynamics (MD) simulations (Figure 1), in order to
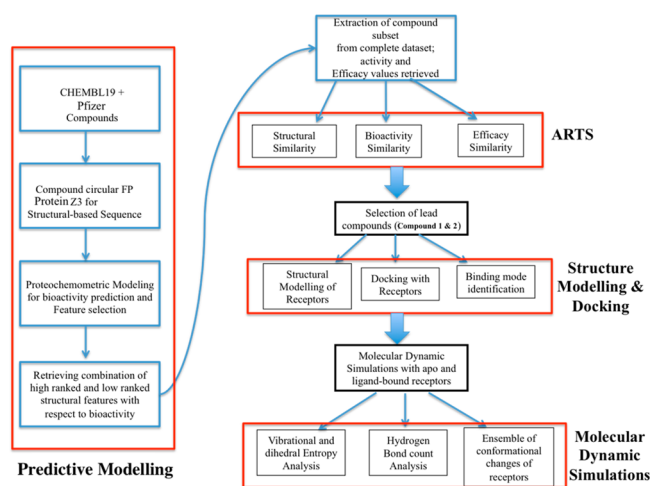

Figure 1. Unified pipeline for the extraction and analysis of receptor subtype-selective compounds used in the study. The workflow utilized predictive modeling approaches, feature selection methods, assay-related similarity assessments, molecular modeling, docking, and molecular dynamics simulations.

develop a hypothesis for compounds binding to the α subunits' interface of GABA receptors. We ultimately hope this work will provide a better understanding of the ligand−receptor interactions that influence functional selectivity, with the aim of improving our ability to develop drugs against this receptor in the future.

MATERIALS AND METHODS

Data Set. The complete data set comprised 5440 compounds from both the ChEMBL19 database[19,20] and the in-house database of Pfizer. Standard bioactivity values used in the model were pK_i values, extracted from ChEMBL as a pChEMBL value, ranging between 4.18 and 10.52 pK_i log units. While retrieving ChEMBL data, a confidence score of 7 or greater was used. In cases where there were more than one activity/efficacy value for a compound, an average value was computed. Activity values from the radio ligand binding assays directly measuring the binding of a compound to the $\alpha 1\gamma 2$ and $\alpha 2\gamma 2$ benzodiazepine binding pocket were extracted from the ChEMBL database.

The binding assays performed by Pfizer had a similar experimental design as that retrieved from ChEMBL[21] and hence were compatible for mixing the binding data. The complete experimental design of the assay is described in the Supporting Information. The bioactivity values of 1221 compounds against the GABA$_A$ $\alpha 1$ and $\alpha 2$ subtypes were extracted from the ChEMBL19 database, out of which 758 compounds were unique. Only 483 ChEMBL compounds had binding activity against both subtypes. Pfizer provided 2100 unique compounds (and a total of 4198 data points) against both subtypes as well. Diazepam was used as a positive control for docking and simulation experiments. Figure 1 explains the workflow of the different approaches used in this study.

Efficacy measurements of compounds against GABA$_A$ $\alpha 1$ and $\alpha 2$ subtypes were retrieved from the ChEMBL19 database and in-house Pfizer database as efficacy percentages calculated by the patch-clamp method.[22] This technique allows the study of single or multiple ion channels in cells. To gain high throughput from these technologies, Pfizer ran a QPatch automated electrophysiology assay.[23] The experimental design of the assays and quality control criteria are explained in detail in the Supporting Information. The efficacy percentage of compounds retrieved from both the ChEMBL and Pfizer data sets was converted to the relative efficacy (RE); that is, the efficacy of each compound was calculated relative to the efficacy of the standard modulator, diazepam (RE$_{diazepam}$ = 1.27 and 1.14 against the $\alpha 1$ and $\alpha 2$ subunits, respectively).

Chemical Structure Preprocessing and Calculation of Chemical and Biological Descriptors. All compounds were standardized by applying the filters "keep large fragments", "neutralize", "remove explicit hydrogens", "clean 2D", and "clean 3D" using JChem standardizer, version 14.11.10.0.[24] After standardization, unhashed circular fingerprints (6519 bits) were generated using RDKit, version 2014.03.1-np18py27_1,[25] and physiochemical properties were calculated using MOE, version 2013.08.[26] A total of 188 2D descriptors were calculated after calculating the partial charges using partial equalization of orbital electronegativities (PEOE).[27] Binding pocket sequences of both aligned subtypes were used to calculate z-scales (first three principal components) of amino acid residues,[28] which were used as target descriptors in PCM models. In addition to z-scales, binary descriptors of proteins were also employed to generate a PCM model. Binary descriptors were defined based on the presence or absence (match or mismatch) of an amino acid in a target. If the amino acid is the same in both targets, then it is given a value of 1; otherwise, it is −1.

Data Preprocessing. Data points were centered to zero mean and scaled to unit variance, followed by removal of columns for which variance was near to zero with the function *nearZeroVar* from the R package *camb*[29] (frequency cutoff = 30/1).
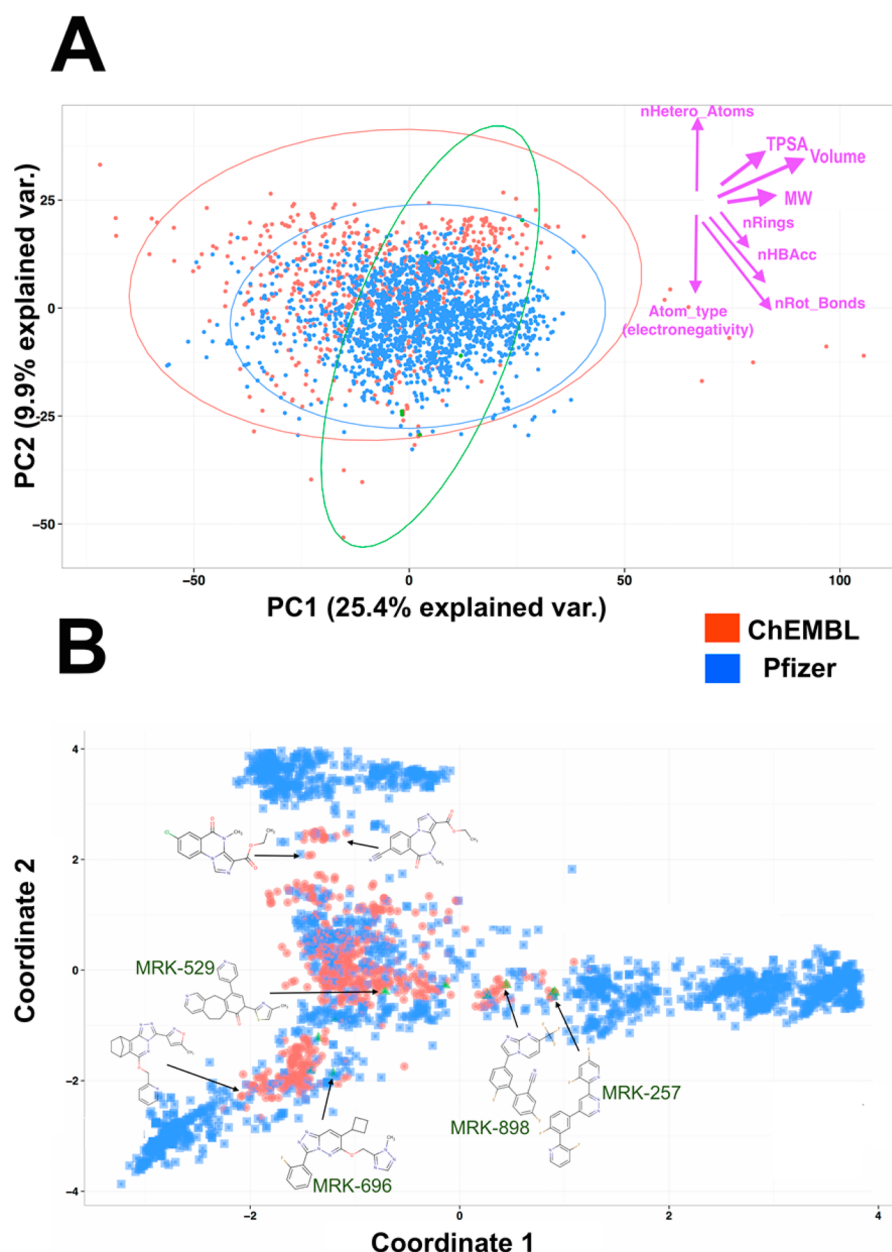
Figure 2. Exploration of chemical space using principal component analysis (PCA) and multidimensional scaling (MDS). (A) PCA of the physicochemical property space of the data sets used in the study including 99% confidence ellipses. The greatest diversity in compounds can be seen in the case of the ChEMBL data set, where larger compounds with large surface areas can be observed on the right-hand side of the figure, whereas smaller compounds can be observed in top left corner. A surprisingly small subset of compounds overlap between the ChEMBL and Pfizer data sets used here, and these compounds belong to the classical benzodiazepines. (B) MDS analysis of structural fingerprints of the data sets. The classical benzodiazepines (overlapping red and blue clusters) and their derivatives overlap the compounds in the center of the plot, whereas imidazopyridine-based molecules are located around it.

Visualization Methods. In order to explore the chemical space of the complete data set, PCA[30] of the physicochemical properties of all molecules was performed using the *princomp* method of the *Stats* package in R-studio, version 0.98.507.[31] PCA ellipses were calculated with a confidence level of 0.99 and plotted using the *ggbiplot* R package.[32] To further explore the similarity of structures of compounds, multi dimensional scaling (MDS)[33] was performed on circular fingerprints in R using the *cmdscale* function. The final matrix was then plotted to identify the similarity and diversity of compounds of the data sets in terms of structure.

Similarity Methods. Structural similarity between compounds was measured using the Tanimoto coefficient by employing the circular fingerprints (256 bits, radius 2) of the compounds. Moreover, the affinity and efficacy similarity was calculated using the assay-related target similarity (ARTS) method. This method employs dose–response measurements of compounds against multiple protein targets to identify the similarity between those targets.[34] ARTS is a quantitative affinity-based similarity index that is based on the hypothesis that two assays applied on two targets are similar if the compounds bind with similar affinity, hence making it an approach for measuring intertarget similarity. The affinity (pK_i) and efficacy (RE) values of compounds against both α subtypes were used to calculate assay-related similarity scores of compounds.

Proteochemometric Modeling (PCM). PCM is an extension of the traditional quantitative structure–activity relationship (QSAR) approach, where, in addition to ligand-based (chemical) features, target similarity in biological space is considered simultaneously.[35,36] In the current work, 6519 Morgan fingerprints of compounds were concatenated with 621 (3 × 207) z-scale and/or 207 binary descriptors of proteins for the complete data set of 5440 ligand–target bioactivity data points. Recursive feature elimination was applied using the 10-fold cross-validation parameter in the *rfeControl* function of the *Caret* package in R. The *rfe* function was then applied on the selected 364 features to keep the most informative features for activity modeling. The features were ranked based on the improvement caused in the fit of the model and the error associated with it. The more improvement observed (and less error), the higher the importance of the feature. Finally, 253 features were selected for model training and testing. Out of 253, 250 were ligand fingerprints and 3 were z-scale protein features.

Model Training. The complete data set was split into 70% training set and 30% test set using the *createDataPartition* function (R *caret* package).[37] Next, 5-fold internal cross-validation was performed on the training data set and predictions were made on the test set. Two machine learning methods, random forest (RF) and decision tree (DT),[38,39] were employed for model training and bioactivity prediction. Random forest was tuned using *mtry* values of 1–8 (R *caret* package), in addition to decision trees (R *rpart* package) using the complexity parameter (*cp*) set equal to zero. The top 253 selected features via RF were used to train a predictive model on the external test set with DT and visualized using the *party* R package.[40−43]

Homology Modeling. The first structure of the GABA$_A$ receptor α1 subtype was modeled in 2012 and was used to hypothesize the common binding modes of traditional benzodiazepines.[44] This structure was used as a template in the current study for modeling the GABA$_A$ receptor α2 subtype. Sequence alignment of the α1 and α2 subtypes, performed by ClustalW,[45] gave about 80% pairwise sequence similarity; hence, this modeled structure of the α1 subtype of the GABA receptor was employed as a template for α2 model prediction using Modeler 9 V3.[46,47] The structures of both α subtypes were aligned by performing structure superimposition using Chimera 1.6[48] and ClustalW, and the root-mean-square deviation (RMSD) was calculated. The homology-modeled structure was evaluated by performing rotamer analysis, assessing DOPE profiles and computing Ramachandran plots as well as G-factor statistics using PROCHECK.[49,50] To calculate the stability of the binding pockets due to the variations in the sequence, the change in energy (ΔG) was calculated between wild type and variants using the FoldX plugin in Yasara.[51]

Docking. Protein structures were prepared using MOE by identifying dominant alternate conformations, adding appropriate disulfide bonds, and adding missing loop regions. Protonate3D was used to assign protonation states considering titration, rotamers, and side chain flips.[52] After the preparation of proteins, each ligand was prepared for docking by adding charges and polar hydrogen atoms in MOE, version 2013.08. The maximum number of docking conformations of each ligand was set to 30 after applying the induced-fit docking protocol of MOE, and the highest ranked (lowest binding energies) conformations were selected.

Molecular Dynamic Simulations. On the basis of the modeled structures of the α1 and α2 subunits and the lowest energy docked poses with ligands, MD simulations were performed to investigate the intrinsic dynamics of the GABA

Table 1. Substructural Features of Compounds Obtained from the Random Forest Feature Selection Approach Related to Affinity against GABA α1 or α2 Subtype[a]

Feature	Structure	Improvement	RMSE
Feature_1557		0.27	0.42
Feature_57		0.19	0.78
Feature_343		0.17	0.42
Featue_527		0.12	0.45
Feature_736		0.076	0.95
Feature_3628		0.068	0.95
Feature_847		0.062	0.95
Feature_56		0.052	0.89
Feature_83		0.014	0.22

[a]The improvement in the bioactivity prediction caused by a feature is given along with the resulting RMSE of the model.

receptor and its change upon ligand binding. Eight independent MD simulations characterizing both receptors in their apo state and as well as in complex with all three ligands using *pmemd* from Amber12[53] were performed. Starting structures were prepared using protonate3D from MOE.[52] Ligands were parametrized using the generalized Amber force field (GAFF)[54] and

AM1-BCC charges;[55] amino acids were described via the Amber force field 99SB-ILDN.[56] All systems were soaked in a truncated octahedral TIP3P solvent box with a minimal wall distance of 10 Å.[57] After employing an elaborate equilibration protocol,[58] all eight systems were sampled for 100 ns each at 300 K and 1 bar, and 10 000 snapshots were saved for later analysis using *cpptraj*.[59]
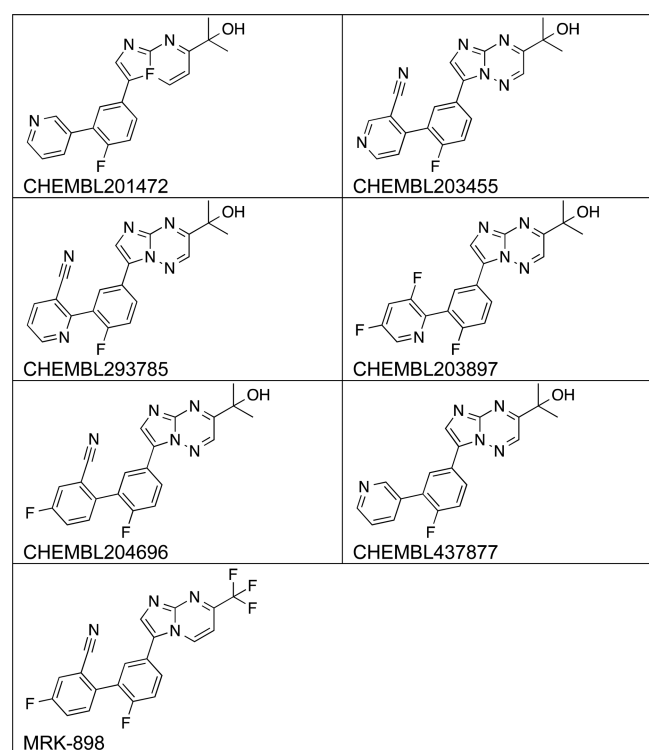

Figure 3. Chemical structures of seven compounds extracted from the data set as subset 1. ChEMBL201472 is known as compound **1** and ChEMBL437877 is known as compound **2** in this study.

After performing standard stability checks for simulations, hydrogen bonding and secondary structure elements involving loop C were analyzed by applying default criteria of *cpptraj* as implemented in AmberTools.[59] Furthermore, the mobility of loop C was characterized by calculating the vibrational entropy from a PCA of its C_α atom positions.[60] The internal dynamics of loop C was also characterized by the calculation of dihedral entropies from residue-wise φ, ψ, and ω backbone torsion distributions.[61] Residue-wise positional fluctuations were captured as global B-factors following alignment of C_α positions and as local B-factors from a residue-wise alignment to the respective backbone atoms.[62]

■ RESULTS AND DISCUSSION

Chemical Space Exploration. All compounds were analyzed on the basis of their physiochemical properties to identify basic properties of allosteric modulators in this space. The PCA explained a total variance of 35% in two components, as shown in Figure 2A, and it can be observed that the compounds have rather distinct physicochemical properties. The most diversity can be seen in the case of the ChEMBL compounds, which have on average high molecular weight and a higher PSA and which are located in the red eclipse. The overlapping subset between the ChEMBL and Pfizer compounds belongs to the classical benzodiazepines chemotype. It can also be seen that the physiochemical properties of all allosteric modulators agree with a recent study by van Westen et al. on the property analysis of (target-independent) allosteric modulators present in the ChEMBL database.[63] In that study, it was found that allosteric modulators to some extent possess different physiochemical properties depending on the target class to which they belong; however, they generally exhibit relatively low molecular weight and high lipophilicity and rigidity.

Furthermore, the allosteric modulators from different sources differ significantly from each other in structural space, as shown in the MDS plot of the chemical fingerprints visualized
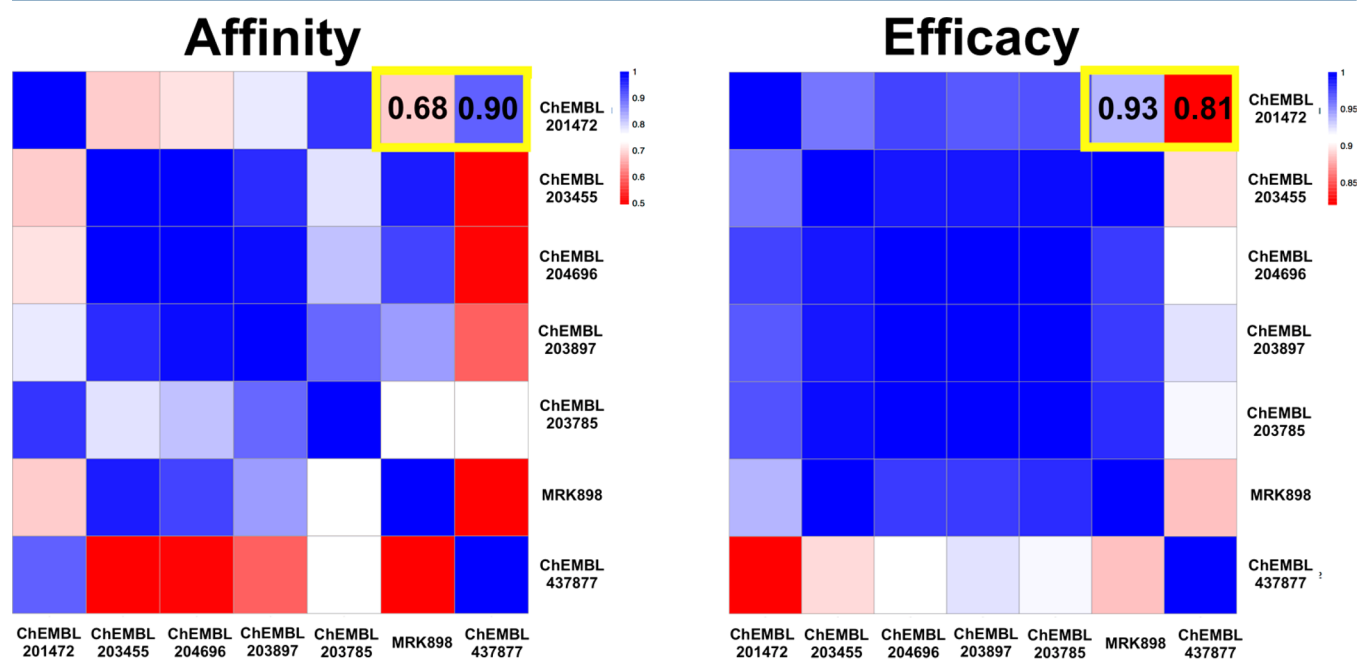

Figure 4. Binding affinity and efficacy similarity of a selected set of GABA modulators. It can be seen that, overall, most of the compounds are similar in bioactivity and efficacy space; however, a few exceptions can be seen in the cases of MRK-898 and compounds **1** and **2** (shown in the yellow box).

in Figure 2B. The Pfizer compounds are shown to form four separate chemotype clusters. The benzodiazepines can again be seen as a large number of compounds that overlap between the Pfizer and ChEMBL compounds in the center of the plot. A small number of overlapping Pfizer compounds can be observed scattered around the main cluster, containing imidazopyridine scaffolds and electronegative atoms in their side chains. Overall, a large diversity of chemical structures is also apparent from the MDS analysis because of the inclusion of a range of chemotypes from both public and internal data sets.

Bioactivity Modeling. The RF bioactivity prediction model trained on 253 features gave a prediction performance of $Q^2_{cv} = 0.64 \pm 0.11$ and $RMSE_{cv} = 0.57 \pm 0.07$ on the internal CV and $R^2_{test} = 0.74$ and $RMSE_{test} = 0.50$ log units on the external test set. The 10-fold CV performance is the mean R^2 of the 10-fold performance of the training data set. Some performed equally as well as the external test set; however, others did not. Since the overall performance was the mean of these, it was observed that it is lower than the performance of the external set. None of the ligand–protein pairs in the training set was present in the test set. However, since the ligands belonging to the Pfizer data set are structurally very similar to each other, this might be responsible for the increased performance of the external test set.

The prediction performances of the benchmarked family and individual QSAR models were measured to be $R^2_{test\_QSAR} = 0.64$ and $RMSE_{QSAR} = 0.58$, $R^2_{test\_\alpha1} = 0.74$ and $RMSE_{test\_\alpha1} = 0.48$, and $R^2_{test\_\alpha2} = 0.57$ and $RMSE_{test\_\alpha2} = 0.60$. The predictive performance of the model generated with binary descriptors of proteins was measured to be $R^2_{binary\_PCM} = 0.69$ and $RMSE_{binary\_PCM} = 0.58$. The performance of the z-scale descriptor model is slightly better than the binary descriptor model; however, the binary model outperforms the benchmarked QSAR model ($R^2_{test\_QSAR} = 0.64$).

The established PCM model (with z-scales) was also compared to individual QSAR models of each target: the performance of the $\alpha1$ QSAR ($R^2_{test\_\alpha1} = 0.74$, $RMSE_{test\_\alpha1} = 0.48$) was comparable to that of our PCM model; however, the $\alpha2$ QSAR ($R^2_{test\_\alpha2} = 0.57$, $RMSE_{test\_\alpha2} = 0.60$) was worse than the benchmarked QSAR as well as the established PCM. Hence, our established PCM model has an improved performance compared to that of the benchmarked family QSAR and individual QSAR (for both targets simultaneously).

The improved performance of PCM models due to the addition of target descriptors was studied previously[64] and hence was a reason for using the z-scales PCM model. Although the z-scales did not add much to the interpretation of the model, they still improved the performance of the PCM model over that of the benchmarked QSAR model ($R^2_{test\_QSAR} = 0.64$) and binary descriptors ($R^2_{test\_PCM} = 0.74$). This improved model generated by employing z-scales was further used for interpretation and selection of features, which resulted in the extraction of subsets of compounds for downstream analysis (which is the main aim of this study). The compounds identified via the feature selection approach also had the desired pharmacological profiles, which increased our confidence in performing model generation and interpretation in a single step (via the PCM approach).

The predictive model was generated on all compounds active against the $\alpha1$ or $\alpha2$ subtype; hence, the selected substructural features help to rationalize (to some extent) the affinity against both receptor subtypes, which will be interpreted below. The top nine substructural features extracted via RF are shown in Table 1. These features are sorted based on their improvement both in the fit of the model and the RMSE.

The Spearman correlation (ρ) between the affinity and efficacy of the compounds was found to be 0.008 and 0.31 against $\alpha1$ and $\alpha2$, respectively. This suggests that there is only a very weak correlation between the affinity and efficacy of GABA$_A$ modulators against both subunits. In other words, the selected features, which were found to be responsible for the affinity of compounds, are unlikely to also explain their efficacy fully. The highest ranking features (given in Table 1) identified four subsets of compounds. Each subset was retrieved based on a combination of different features from Table 1. The first subset consisted of seven compounds with a Spearman correlation between affinity and efficacy of −0.33 ($\alpha1$) and −0.94 ($\alpha2$). The presence of feature_57, feature_343, and feature_527 from Table 1 is evident in the structures of compounds in subset 1 (Figure 3). The second subset (159 Pfizer compounds) had a Spearman correlation between affinity and efficacy of −0.144 against both subtypes. The third (17 Pfizer compounds) and fourth (8 ChEMBL compounds) subsets of compounds had no reported functional value and hence were not used further. Feature_1557, feature 3682, feature_56, and feature_847 from Table 1 were observed in compounds from subsets 2 and 3; however, the structures of these compounds were not added in this article.

This relationship was further investigated using a case study of seven compounds (ChEMBL201472, ChEMBL203455, ChEMBL204696, ChEMBL203897, ChEMBL203785, MRK898, and ChEMBL437877) from the above-mentioned subsets based on the presence of the top selected features (the structures of these compounds are shown in Figure 3) . Overall, most of these compounds showed similarities in structure and affinity but not in efficacy (Figure 4).

In the following, we will now consider a pair of compounds, ChEMBL201472 (from here on called compound **1**) and ChEMBL437877 (compound **2**) because of their high similarity in structure and affinity, but not in efficacy, in order to develop a model for the underlying drivers of affinity and efficacy of GABA$_A$ modulators. The structure, affinity, and efficacy of compounds **1** and **2** and diazepam are given in Supporting Information Figure S1. Moreover, we will (a) investigate their pharmacological profile as compared to that of other compounds in the subset and (b) investigate their functional differences via structure-based methods, namely, docking and MD simulations.

MRK-898 was found to be the closest relative of compounds **1** and **2** in terms of structure (Tanimoto coefficients of 0.997 and 0.994, respectively). Both compounds contain an identical main scaffold (imidazopyrimidine), although their side chains differ. When this small difference in molecular structure is mapped in terms of their affinity and efficacy (Figure 4), compound **1** showed similarity to compound **2** (0.90) in bioactivity space but not to MRK-898 (0.93) in terms of efficacy. The remaining four compounds (ChEMBL203897, ChEMBL203785, ChEMBL203455, and ChEMBL204696) have similar scaffolds (imidazopyrazine) to compound **2** but differ only in their side chains. The relationships among compounds **1**, **2**, and MRK-898 showed that the change in the scaffold does not satisfactorily explain the observed affinity and efficacy trends and also indicated that side chains need to be considered in more detail. Hence, structural analysis was performed in the next step.

Homology Modeling of GABA$_A$ $\alpha2$ Subtype Receptor. We first established a model of the GABA$_A$ $\alpha2$ subtype receptor and examined its reliability as follows. The modeled $\alpha2\gamma2$ structure was superimposed with $\alpha1\gamma2$, and the resulting RMSD of 0.51 Å suggested a very close resemblance between the
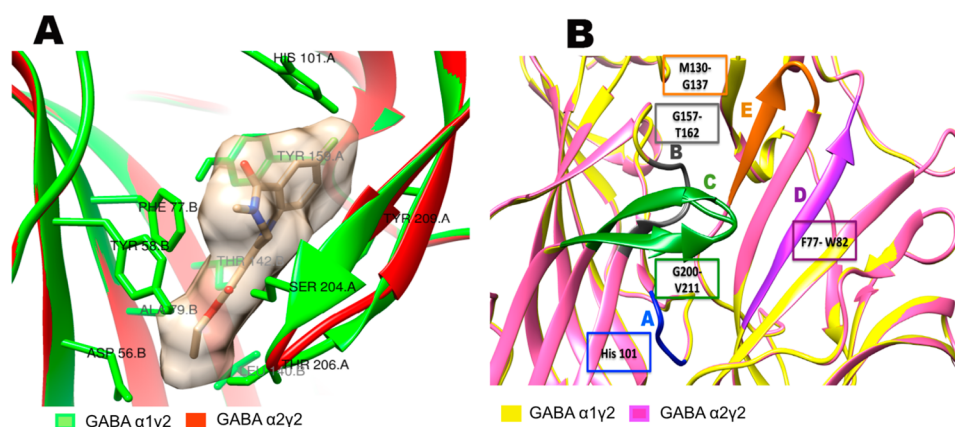
Figure 5. (A) Superimposed structures of the GABA $\alpha1\gamma2$ and $\alpha2\gamma2$ complexes with the classical benzodiazepine flunitrazepam docked into the benzodiazepine binding pocket. Interacting residues from the α subunit (His-101, Tyr-159, Tyr-209, and Thr-206) and the γ subunit (Phe-77, Thr-142, Leu-140, and Asp-56) are shown as sticks. (B) Superimposed benzodiazepine binding pocket of the GABA $\alpha1\gamma2$ and $\alpha2\gamma2$ complexes with annotated loops (A, B, C, D, and E). The amino acids included in each loop are also indicated in the boxes. It can be seen that there are no structural differences in loops A and B; however, a significant conformational change can be observed in loop C (see the main text for a more detailed description and discussion).

structures of both proteins. Rotamer analysis showed unordered side chains of the modeled structures, which were corrected using the Dunbrack backbone-dependent rotamer library.[65] The DOPE profile (Supporting Information Figure S2) showed a stable energy per residue of the modeled structures except for residues 35−40 and 85−90, where the DOPE score was greater than −0.03 and −0.02, respectively. PROCHECK statistics showed that 86.8% of the residues were in the most favored regions and that 1.1% were in the disallowed regions of the Ramachandran plot (Supporting Information Figure S3). The overall average G-factor of the modeled structure was calculated to be −0.20, indicating that the model is reasonable.

On the basis of this model, we next investigated the benzodiazepine binding pocket of both complexes in order to visualize their structural differences. The benzodiazepine binding pocket (Figure 5A) is composed of five loops,[66] three which (A, B, and C) are part of the α subunit, whereas loops D and E are part of the γ subunit. The structural alignment of the $\alpha1$ and $\alpha2$ binding pockets with annotated loops is given in Figure 5B and Supporting Information Figure S4. It can be seen that loop A is identical in the $\alpha1$ and $\alpha2$ subtypes, whereas two substitutions in loop B and eight substitutions in loop C were identified. No significant changes in the structure of loop B were found because of these variations; however, a significant shift in loop C was observed. Hence, we hypothesized that this conformational change in the protein structure might be responsible for the differences in the binding modes of GABA$_A$ modulators and hence their efficacy, particularly because mutational studies of these residues (Ser-204, Val-202, and Tyr-209) of loop C suggested that these variations are known to affect the activity of benzodiazepines.[66−69]

Compound Docking Experiments. We next performed docking experiments in order to identify and investigate the binding modes of compounds **1** and **2** with both the $\alpha1$ and $\alpha2$ subtypes. The binding mode of the two compounds with the $\alpha1$ subtype showed the following interactions: (a) His-101 of the GABA$_A$ $\alpha1$ subtype interacted with both compounds during docking experiments (Figure 6A) and (b) PLIFs identified many loop C residues as major participants of both series of docking experiments, namely, Tyr-159, Tyr-209, and Ser-204, in addition to Thr-142 and Phe-77 of the γ chain, as also
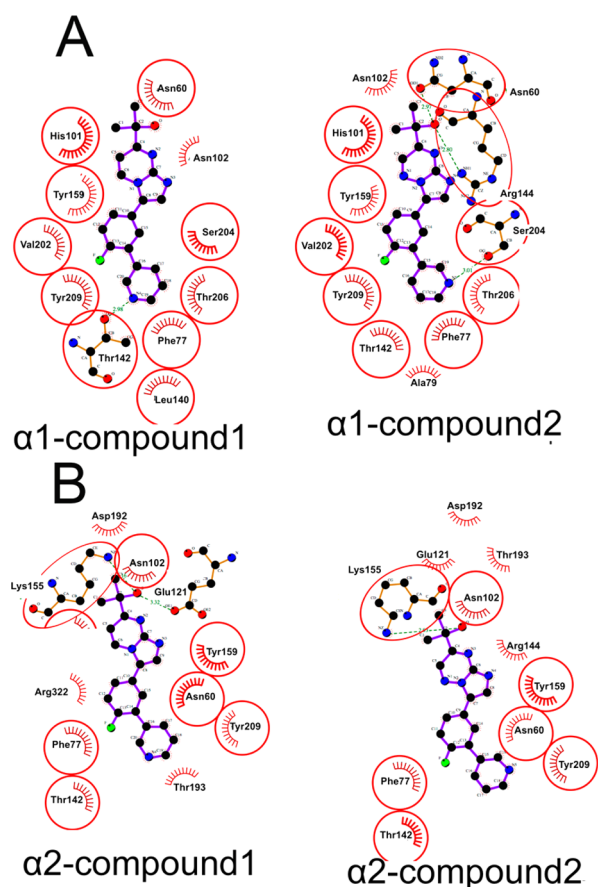

Figure 6. Ligplots[72] of docked complexes of compounds **1** and **2** with the (A) $\alpha1$ and (B) $\alpha2$ subtypes. All residues encircled in red were found to be common between the two complexes. Hydrogen bonds are shown with a green dotted line. The characteristic His-101 interaction is evident in the $\alpha1$ dockings. The added hydrogen bonds between the side chain oxygen and Asn-60 and Arg-144 were seen due to the displacement in the binding mode because of the additional nitrogen in compound **2**. A flip of the pyridine ring is also observed in compound **2**, leading to an interaction of Ser-204 with $\alpha1$. Hence, the binding modes of the compounds against the $\alpha1$ subtype agree with the literature, and there are novel interactions identified in the case of $\alpha2$.

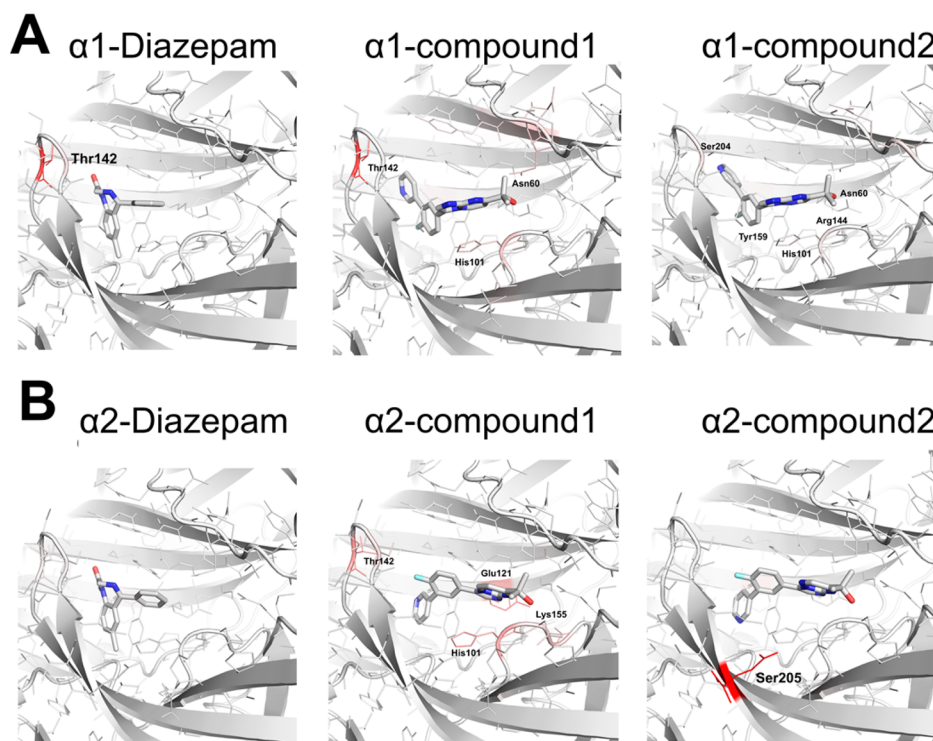**Figure 7.** Binding poses of diazepam and compounds **1** and **2** with the (A) α1 and (B) α2 subunits. Hydrogen bonds are colored in red. More hydrogen bonds were observed in compound **1** and diazepam against both receptors as compared to compound **2**. The stacking between ligands with His-101 and the fluorobenzyl group with Tyr-159 and Tyr-209 is observed against α1, whereas these conformations are disturbed in the case of α2 complexes. These results are explained in more detail in the simulation section. Hence, overall, a large number of hydrogen bonds were observed in the α2 subtype–ligand complex as compared to α1 due to variations in loop C.

observed previously.[66] These interactions agreed with the common binding modes (CBM-I) of classical benzodiazepines with the α1 binding pocket as studied previously.[44] From these observations, the finding that the interaction of His-101 with the compounds is selective to α1 dockings/binding is consistent with earlier findings.[7,70,71] However, only in the case of diazepam was His-101 found to be important in both the α1 and α2 docking poses, which might be because diazepam is a full agonist for both the α1 and α2 subtypes (RE$_{α1}$ = 1.27, RE$_{α2}$ = 1.14). Loop C residues (Gly-200, Val-202, and Ser-204) were also observed in interactions of both the α1 and α2 docked complexes, which is consistent with earlier findings.[66] The conformational changes in this loop might lead to a change in the binding mode of the compounds, which was explored further in the MD section. Moreover, it was observed that Tyr-159 and Tyr-209 form stacking interactions with the side chains, in addition to His-101 π–π interactions with the main scaffold, in the case of compounds **1** and **2** binding to α1 (Figure 6A). In addition to this, Thr-142, Asn-60, and Arg-144 of the γ chain of the α1 subtype were observed to form strong hydrogen bonds with the heterocyclic groups of compounds **1** and **2**. In the binding of compounds with the α2 subtype, the following observations were made: (a) No interaction with His-101 was observed and (b) interactions with loop C residues were disturbed and the pocket groove was distorted. The interactions were shifted from Asn-60 and Arg-144 toward Asn-102 and Lys-155 of the γ chain (Figure 6B). Moreover, the classic stacking interaction of compounds with two tyrosines was also disturbed in the α2 docking poses.

The additional nitrogen atom in the scaffold of compound **1** relative to that of compound **2** was expected to interact

differently, which is indeed what we observed, resulting in additional hydrogen bonds between the side chain oxygen and Asn-60 and Arg-144, along with a hydrogen bond with Ser-204 (Figure 6).

Influence of Amino Acid Variations (G200E and I201T) on Binding Energy in the α2 Subtype. A difference of eight amino acids was identified in loop C between the α1 and α2 subtypes during the structural alignment of both binding pockets. These amino acid variations in the loop C region of the α2 subtype can affect the stability of the binding pocket and hence the common binding modes of compounds. In order to calculate the stability of the binding pocket due to these substitutions, mutation stability analysis was performed to calculate the change in the energy of stabilization (ΔG) between the wild-type (WT) and variant (VT) subtypes. Out of eight variations, only two were found to be destabilizing. These destabilizing variations in α2 were G200E and I201T (Supporting Information Figure S5), with ΔG values of +0.83 and +1.19 kcal/mol, respectively.

Flexibility Analysis of the Apo α2 Binding Pocket. To understand the effect of these variations on both α subunits, the conformational changes taking place in the loop C region of the α2 subtype were identified from a 100 ns MD simulation (Figure 7), leading to the following observations (Supporting Information Figure S6): (a) The α1 subtype was found to be more flexible than the α2 subtype both globally and locally at loop C, (b) a higher B-factor was observed in the case of the α1 subtype in both local and global alignments, suggesting a higher entropy and more flexibility in the α1 subtype than in the α2 subtype of the GABA receptor, and (c) a higher number of hydrogen bonds and increase in secondary structure content were observed in the α2 subtype as compared to the α1 subtype.
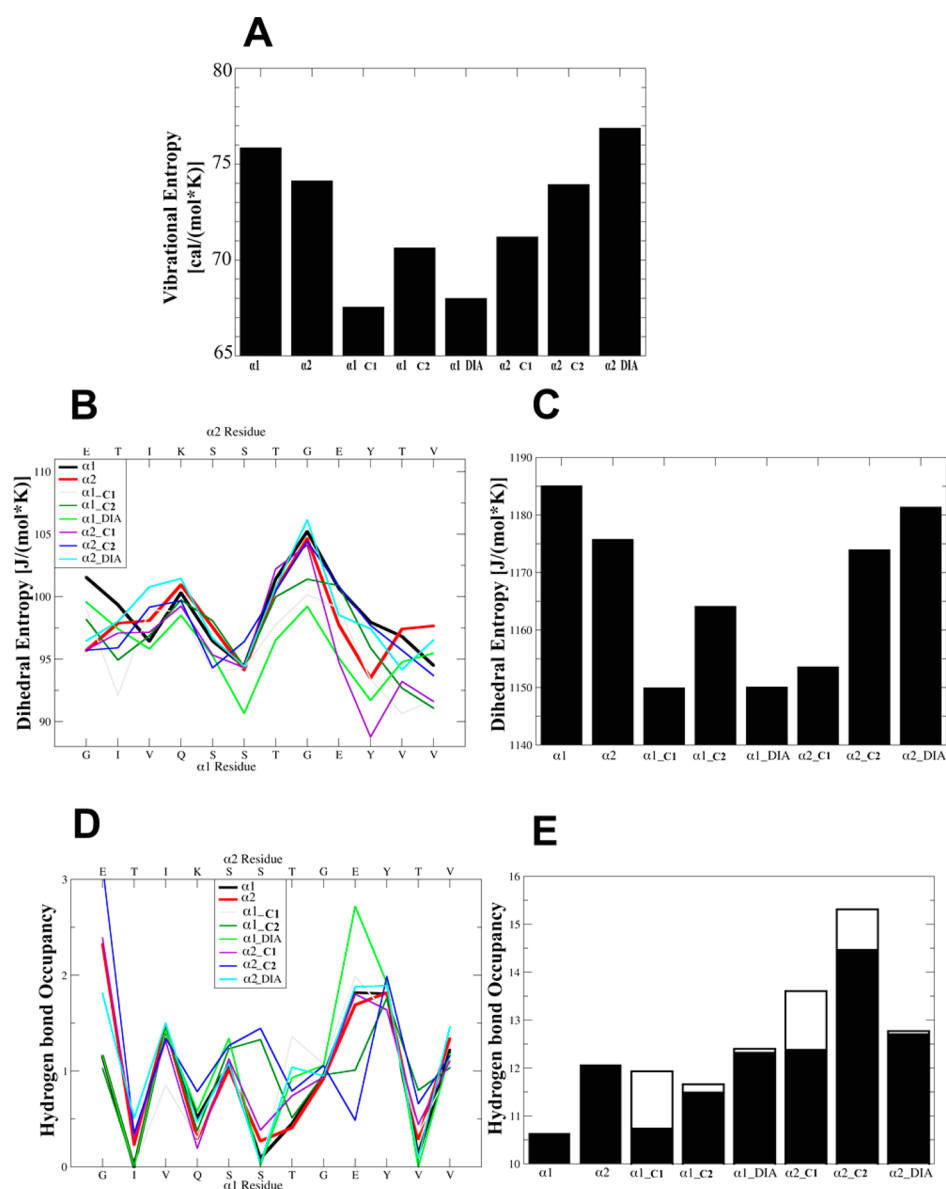
Figure 8. Molecular dynamics and simulation results. (A) Vibrational entropy of $\alpha1$ and $\alpha2$ subtypes with compound **1** (labeled C1) and compound **2** (labeled C2), in addition to diazepam (positive control). (B) Residue-wise dihedral entropy of the loop C region of the GABA $\alpha1$ and $\alpha2$ subtypes with and without ligand bound (compounds **1** and **2** and diazepam). (C) Overall dihedral entropy of both subtypes and their ligand-bound complexes. The decreased entropy of the $\alpha2$ subtype in its apo state as compared to the $\alpha1$ subtype is because of the presence of stabilizing amino acid variations in loop C. An entropy increase was observed in the ligand-bound state for both subtypes; however, the increase was more pronounced for $\alpha2$ compared to the $\alpha1$ subtype. (D) Residue-wise hydrogen bond occupancy of the loop C region of the $\alpha1$ and $\alpha2$ subtypes with and without bound ligand (compounds **1** and **2** and diazepam). (E) Total hydrogen bond counts of $\alpha1$ and $\alpha2$ subtypes with and without bound ligand. With the amino acid variations in the loop C region, the $\alpha2$ subtype gained a higher number of hydrogen bonds. However, when bound to a ligand, the $\alpha1$ subtype showed more interactions than the $\alpha2$ subtype. Hence, the increases in entropy and number of hydrogen bonds in the $\alpha2$−ligand bound state might be key features related to the increased efficacy of compound **2**.

All of these observations led to the conclusion that the $\alpha2$ subtype became more rigid than the $\alpha1$ subtype because of these variations, namely, Gly-200 to Glu-200, Ile-201 to Thr-201, and Val-202 to Ile-202, and had an increased number of side chain internal contacts compared to the $\alpha1$ subtype (see Supporting Information Figure S5 for more details).

Ligand Bound and Unbound MD Simulations and Vibrational Entropy Analysis. An extensive vibrational entropy analysis was next performed for the ligand-bound protein complexes in order to relate the difference in functional activity of compounds **1** and **2** (with compound **2** being significantly more efficacious against $\alpha2$ than compound **1**) with the

differences in their binding behavior to the $\alpha1$ and $\alpha2$ subtypes. The vibrational entropy of C_α was hence calculated for protein complexes with and without ligand bound, the result of which is visualized in Figure 8A. It can be observed that the $\alpha1$ subtype is more flexible (higher entropy) than the $\alpha2$ subtype without a ligand bound; however, this flexibility decreased upon ligand binding. Although the increased entropy of the $\alpha1$ subtype as compared to $\alpha2$ was expected from results shown previously, the decrease in entropy upon ligand binding suggests a higher entropy loss upon ligand binding to the $\alpha1$ subtype. Interestingly, the observed conformational freezing was seen to be much larger in the case of the $\alpha1$ subtype than $\alpha2$ for both compounds **1**

and 2, leading to a maximum flexibility in the case of compound **2** binding to the $\alpha 2$ subtype of the GABA receptor. Here, this difference in intrinsic flexibility could be one of the reasons for the increased functional signal in the case of $\alpha 2$ for compound **2**; in other words, the least entropy is lost upon forming this particular ligand−target interaction.

Dihedral Entropy Analysis of the Ligand-Bound State. Given that protein backbone dihedral angles are significant determinants of the conformational entropy of molecules, dihedral entropies were next calculated for each residue of both proteins (visualized in Figure 8B). It was found that overall higher entropies were associated with disordered regions. Gly-200 in loop C was responsible for the higher entropy of the $\alpha 1$ apo structure than the $\alpha 2$ apo structure, which contains Glu-200 (Figure 8B). The entropies of both subtypes were seen to decrease in their ligand-bound states (freezing of the loop); however, a decrease in entropy was observed more in the ligand-bound $\alpha 1$ subtype. Similar inferences were made after observing the residue-wise contribution of total entropy (Figure 8C).

Hydrogen Bond Analysis of Complexed Structures. We next analyzed the enthalpic contributions to binding by performing hydrogen bond analyses. The per-residue hydrogen bond occupancy of both the $\alpha 1$ and $\alpha 2$ subtypes is visualized in Figure 8D. The hydrogen bonds calculated after a 100 ns simulation showed why the Gly-200 to Glu-200 substitution had a large impact on the flexibility of $\alpha 2$, namely, by forming 0.8 hydrogen bonds on average in the former case and 2.2 in the latter. Similar kinds of losses and gains of hydrogen bonds were observed in the cases of the ligand-bound $\alpha 1$ and $\alpha 2$ structures. The Gln-203 to Lys-203 substitution added more hydrogen bonding interactions for $\alpha 2$−compound **2** as compared to $\alpha 2$−compound **1**. Moreover, hydrogen bond counts in both complexes were analyzed, the result of which is visualized in Figure 8E. In the apo state, $\alpha 1$ has a lower number of total hydrogen bonds than $\alpha 2$. The increased number of hydrogen bonds in the $\alpha 2$ subtype could be because of sequence variations. In the case of the ligand-bound $\alpha 1$ and $\alpha 2$ subtypes, a gain in the total number of hydrogen bonds in absolute terms was observed. The increase in hydrogen bonding was observed more in the $\alpha 2$ subtype than $\alpha 1$ with both compounds. Here, to our surprise, compound **2** gained fewer total hydrogen bonds than compound **1** against both subtypes, despite the presence of an additional nitrogen. This suggests that compound **2** preferentially binds to the solvent instead of the receptor (both subtypes). Despite its binding to the solvent, compound **2** was observed to make enough interactions with the $\alpha 2$ subtype (compared to $\alpha 1$) to elicit a functional response, which could be a possible answer to the increased efficacy of compound **2** against $\alpha 2$.

CONCLUSIONS

In this study, we devised and implemented an analysis of GABA$_A$ (receptor) modulators to understand their affinity and efficacy profiles against the $\alpha 1$ and $\alpha 2$ subtypes. We used our workflow on the GABA receptor $\alpha 1$ and $\alpha 2$ subtypes by combining modulators from public and proprietary data sets, and we performed the proposed analysis to correlate their affinity and efficacy profiles. The analysis showed a very weak correlation between the affinity and efficacy of the compounds (0.008 and 0.31 against the $\alpha 1$ and $\alpha 2$ subtypes, respectively). Next, feature selection approaches were employed to obtain substructural features associated with affinity (and not with efficacy), which were further used to select a subset of compounds with different profiles in structural space, affinity space, and efficacy space.

Two of the compounds (compounds **1** and **2**) were then used for further analysis in order to identify the differences in their binding modes associated with affinity and efficacy.

Compounds **1** and **2** were found to be structurally very similar (except for the additional nitrogen in the case of compound **2**), but they showed different functional profiles, which we attempted to further elucidate via structure-based modeling approaches. When docked with both the $\alpha 1$ and $\alpha 2$ subtypes, it was found that the ligand−protein interactions of compounds **1** and **2** differed considerably. We found that the substitutions of Gly-200, Ile-201, and Val-202 in the $\alpha 1$ subtype to Glu-200, Thr-201 and Ile-202 in the $\alpha 2$ subtype were responsible for increased rigidity and internal hydrogen bonding in the latter structure. These results were further confirmed by vibrational and dihedral entropy and hydrogen bond occupancy analyses, where it was found that the above-mentioned substitutions resulted in a higher entropy (increased rigidity) in the $\alpha 2$ subtype along with a loss of hydrogen bond interactions with its ligands, leading to a higher efficacy of compound **2** against $\alpha 2$ as compared to $\alpha 1$ subtype (for detailed conformational analysis, see Supporting Information Figure S7).

Hence, by considering enthalpic and entropic contributions to binding to the $\alpha 1$ and $\alpha 2$ subtypes of the GABA receptor, based on ligand- and structure-based analyses, we were able to develop hypotheses for functional selectivity of ligands for those subtypes. We hope that this study will contribute to the design of more efficacious and selective modulators of this receptor. The analysis methods applied here are also generally applicable for designing receptor subtype-selective compounds where affinity and efficacy show little correlation.

ASSOCIATED CONTENT

AUTHOR INFORMATION

Corresponding Authors
*E-mail: Julian.Fuchs@uibk.ac.at (J.E.F.).
*E-mail: ab454@cam.ac.uk (A.B.).

Present Address
∥(J.E.F.) Department of Medicinal Chemistry, Boehringer Ingelheim RCV GmbH & Co KG, Dr. Boehringer Gasse 5-11, 1120 Vienna, Austria.

Author Contributions
Participated in research design: Qurrat Ain, Andreas Bender, David Pryde, Robert Owen, Kiyoyuki Omoto, and Krishna C. Bulusu. Conducted experiments: Qurrat Ain and Julian Fuchs. Performed analysis: Qurrat Ain, Julian Fuchs, and Rubben Torella. Wrote and contributed to the manuscript: Qurrat Ain, Andreas Bender, David Pryde, Robert Owen, Kiyoyuki Omoto, Julian Fuchs, Rubben Torella, and Robert Glen.

Notes
The authors declare no competing financial interest.

ACKNOWLEDGMENTS

■ REFERENCES

(1) Reynolds, A.; Brustein, E.; Liao, M.; Mercado, A.; Babilonia, E.; Mount, D.; Drapeau, P. Neurogenic Role of the Depolarizing Chloride Gradient Revealed by Global Overexpression of KCC2 from the Onset of Development. *J. Neurosci.* **2008**, *28*, 1588−1597.

(2) Rudolph, U.; Knoflach, F. Beyond Classical Benzodiazepines: Novel Therapeutic Potential of GABAA Receptor Subtypes. *Nat. Rev. Drug Discovery* **2011**, *10*, 685−697.

(3) McCarson, K.; Enna, S. GABA Pharmacology: The Search for Analgesics. *Neurochem. Res.* **2014**, *39*, 1948−1963.

(4) Brickley, S. G.; Mody, I. Extrasynaptic GABA(A) Receptors: Their Function in the CNS and Implications for Disease. *Neuron* **2012**, *73*, 23−34.

(5) Whiting, P. J. GABA-A Receptor Subtypes in the Brain: A Paradigm for CNS Drug Discovery? *Drug Discovery Today* **2003**, *8*, 445−450.

(6) Olsen, R. W.; Delorey, T. GABA Receptor Physiology and Pharmacology. *Basic Neurochem. 6th Ed. Mol. Cell. Med. Asp* **1999**, 10−12.

(7) Sigel, E.; Steinmann, M. E. Structure, Function, and Modulation of GABA(A) Receptors. *J. Biol. Chem.* **2012**, *287*, 40224−40231.

(8) Reddy, D. S. Neurosteroids: Endogenous Role in the Human Brain and Therapeutic Potentials. *Prog. Brain Res.* **2010**, *186*, 113−137.

(9) Atack, J. R. Anxioselective Compounds Acting at the GABA(A) Receptor Benzodiazepine Binding Site. *Curr. Drug Targets: CNS Neurol. Disord.* **2003**, *2*, 213−232.

(10) Atack, J. R.; Hallett, D. J.; Tye, S.; Wafford, K.; Ryan, C.; Sanabria-Bohórquez, S. M.; Eng, W.-S.; Gibson, R. E.; Burns, H. D.; Dawson, G. R.; Carling, R. W.; Street, L. J.; Pike, A.; De Lepeleire, I.; Van Laere, K.; Bormans, G.; de Hoon, J. N.; Van Hecken, A.; McKernan, R. M.; Murphy, M. G.; Hargreaves, R. J. Preclinical and Clinical Pharmacology of TPA023B, a GABAA Receptor $\alpha2/\alpha3$ Subtype-Selective Partial Agonist. *J. Psychopharmacol.* **2011**, *25*, 329−344.

(11) Rudolph, U.; Crestani, F.; Benke, D.; Brünig, I.; Benson, J. A.; Fritschy, J. M.; Martin, J. R.; Bluethmann, H.; Möhler, H. Benzodiazepine Actions Mediated by Specific Gamma-Aminobutyric acid(A) Receptor Subtypes. *Nature* **1999**, *401*, 796−800.

(12) McKernan, R. M.; Rosahl, T. W.; Reynolds, D. S.; Sur, C.; Wafford, K. A.; Atack, J. R.; Farrar, S.; Myers, J.; Cook, G.; Ferris, P.; Garrett, L.; Bristow, L.; Marshall, G.; Macaulay, A.; Brown, N.; Howell, O.; Moore, K. W.; Carling, R. W.; Street, L. J.; Castro, J. L.; Ragan, C. I.; Dawson, G. R.; Whiting, P. J. Sedative but Not Anxiolytic Properties of Benzodiazepines Are Mediated by the GABA(A) Receptor alpha1 Subtype. *Nat. Neurosci.* **2000**, *3*, 587−592.

(13) Atack, J. R. The Benzodiazepine Binding Site of GABA(A) Receptors as a Target for the Development of Novel Anxiolytics. *Expert Opin. Invest. Drugs* **2005**, *14*, 601−618.

(14) Atack, J. R. GABAA Receptor Subtype-Selective Modulators. I. $\alpha2/\alpha3$-Selective Agonists as Non-Sedating Anxiolytics. *Curr. Top. Med. Chem.* **2011**, *11*, 1176−1202.

(15) Atack, J. R. GABAA Receptor Subtype-Selective Modulators. II. $\alpha5$-Selective Inverse Agonists for Cognition Enhancement. *Curr. Top. Med. Chem.* **2011**, *11*, 1203−1214.

(16) Atack, J. R. GABAA Receptor Subtype-Selective Efficacy: TPA023, an $\alpha2/\alpha3$ Selective Non-Sedating Anxiolytic and $\alpha5$IA, an $\alpha5$ Selective Cognition Enhancer. *CNS Drug Rev.* **2008**, *14*, 25−35.

(17) Atack, J. R. Subtype-Selective GABA(A) Receptor Modulation Yields a Novel Pharmacological Profile: The Design and Development of TPA023. *Adv. Pharmacol.* **2009**, *57*, 137−185.

(18) Atack, J. R.; Monti, J. M. Development of Subtype-Selective GABAA Receptor Compounds for the Treatment of Anxiety, Sleep Disorders and Epilepsy. *GABA and Sleep* **2010**, 25−72.

(19) Gaulton, A.; Bellis, L. J.; Bento, A. P.; Chambers, J.; Davies, M.; Hersey, A.; Light, Y.; McGlinchey, S.; Michalovich, D.; Al-Lazikani, B.; Overington, J. P. ChEMBL: A Large-Scale Bioactivity Database for Drug Discovery. *Nucleic Acids Res.* **2012**, *40*, D1100−D1107.

(20) Bento, A. P.; Gaulton, A.; Hersey, A.; Bellis, L. J.; Chambers, J.; Davies, M.; Krüger, F. A.; Light, Y.; Mak, L.; McGlinchey, S.; Nowotka, M.; Papadatos, G.; Santos, R.; Overington, J. P. The ChEMBL Bioactivity Database: An Update. *Nucleic Acids Res.* **2014**, *42*, D1083−D1090.

(21) Kahnberg, P.; Lager, E.; Rosenberg, C.; Schougaard, J.; Camet, L.; Sterner, O.; Nielsen, E.; Nielsen, M.; Liljefors, T. Refinement and Evaluation of a Pharmacophore Model for Flavone Derivatives Binding to the Benzodiazepine Site of the GABA(A) Receptor. *J. Med. Chem.* **2002**, *45*, 4188−4201.

(22) Madsen, C.; Jensen, A. A.; Liljefors, T.; Kristiansen, U.; Nielsen, B.; Hansen, C. P.; Larsen, M.; Ebert, B.; Bang-Andersen, B.; Krogsgaard-Larsen, P.; Frølund, B. 5-Substituted Imidazole-4-Acetic Acid Analogues: Synthesis, Modeling, and Pharmacological Characterization of a Series of Novel Gamma-Aminobutyric acid(C) Receptor Agonists. *J. Med. Chem.* **2007**, *50*, 4147−4161.

(23) Liu, Y.; Mathes, C.; Friis, S.; Finley, M. QPatch: The Missing Link between HTS and Ion Channel Drug Discovery. *Comb. Chem. High Throughput Screening* **2009**, *12*, 78−95.

(24) *JChem Standardizer*: Structure Canonicalization and More, 2013.

(25) Landrum, G. *RDKit*: Open-Source Cheminformatics, 2011.

(26) *Molecular Operating Environment (MOE)*, 2013.08, 2013.

(27) Gasteiger, J.; Marsili, M. Iterative Partial Equalization of Orbital Electronegativity—a Rapid Access to Atomic Charges. *Tetrahedron* **1980**, *36*, 3219−3228.

(28) Sandberg, M.; Eriksson, L.; Jonsson, J.; Sjöström, M.; Wold, S. New Chemical Descriptors Relevant for the Design of Biologically Active Peptides. A Multivariate Characterization of 87 Amino Acids. *J. Med. Chem.* **1998**, *41*, 2481−2491.

(29) Murrell, D. S.; Cortes-Ciriano, I.; van Westen, G. J. P.; Stott, I. P.; Malliavin, T.; Bender, A.; Glen, R. C. Chemically Aware Model Builder (Camb): An R Package for Property and Bioactivity Modelling of Small Molecules. *J. Cheminf.* **2015**, *7*, 45. http://github.com/cambDI/camb

(30) Abdi, H.; Williams, L. J. Principal Component Analysis. *Wiley Interdiscip. Rev. Comput. Stat.* **2010**, *2*, 433−459.

(31) *R: A Language and Environment for Statistical Computing*, 2015.

(32) Vincent, Q. V. *Ggbiplot*: A ggplot2 Based Biplot, 2011.

(33) Bronstein, A. M.; Bronstein, M. M.; Kimmel, R. Generalized Multidimensional Scaling: A Framework for Isometry-Invariant Partial Surface Matching. *Proc. Natl. Acad. Sci. U. S. A.* **2006**, *103*, 1168−1172.

(34) Bieler, M.; Heilker, R.; Köppen, H.; Schneider, G. Assay Related Target Similarity (ARTS) - Chemogenomics Approach for Quantitative Comparison of Biological Targets. *J. Chem. Inf. Model.* **2011**, *51*, 1897−1905.

(35) van Westen, G. J. P.; Wegner, J. K.; IJzerman, A. P.; van Vlijmen, H. W. T.; Bender, A. Proteochemometric Modeling as a Tool to Design Selective Compounds and for Extrapolating to Novel Targets. *MedChemComm* **2011**, *2*, 16−30.

(36) Cortés-Ciriano, I.; Ain, Q. U.; Subramanian, V.; Lenselink, E. B.; Méndez-Lucio, O.; IJzerman, A. P.; Wohlfahrt, G.; Prusis, P.; Malliavin, T. E.; van Westen, G. J. P.; Bender, A. Polypharmacology Modelling Using Proteochemometrics (PCM): Recent Methodological Developments, Applications to Target Families, and Future Prospects. *MedChemComm* **2015**, *6*, 24−50.

(37) Kuhn, M. Building Predictive Models in R Using the Caret Package. *J. Stat. Softwre* **2008**, *28*, 1.

(38) Breiman, L. Random Forests. *Mach. Learn.* **2001**, *45*, 5−32.

(39) Quinlan, J. R. Introduction of Decision Trees. *Mach. Learn.* **1986**, *1*, 81−106.

(40) Garge, N. R.; Bobashev, G.; Eggleston, B. Random Forest Methodology for Model-Based Recursive Partitioning: The mobForest Package for R. *BMC Bioinf.* **2013**, *14*, 125.

(41) Strobl, C.; Boulesteix, A.-L.; Kneib, T.; Augustin, T.; Zeileis, A. Conditional Variable Importance for Random Forests. *BMC Bioinf.* **2008**, *9*, 307.

(42) Strobl, C.; Boulesteix, A.-L.; Zeileis, A.; Hothorn, T. Bias in Random Forest Variable Importance Measures: Illustrations, Sources and a Solution. *BMC Bioinf.* **2007**, *8*, 25.

(43) Hothorn, T.; Hornik, K.; Zeileis, A. Unbiased Recursive Partitioning: A Conditional Inference Framework. *J. Comput. Graph. Stat.* **2006**, *15*, 651−674.

(44) Richter, L.; de Graaf, C.; Sieghart, W.; Varagic, Z.; Mörzinger, M.; de Esch, I. J. P.; Ecker, G. F.; Ernst, M. Diazepam-Bound GABAA Receptor Models Identify New Benzodiazepine Binding-Site Ligands. *Nat. Chem. Biol.* **2012**, *8*, 455−464.

(45) Larkin, M. A.; Blackshields, G.; Brown, N. P.; Chenna, R.; McGettigan, P. A.; McWilliam, H.; Valentin, F.; Wallace, I. M.; Wilm, A.; Lopez, R.; Thompson, J. D.; Gibson, T. J.; Higgins, D. G. Clustal W and Clustal X version 2.0. *Bioinformatics* **2007**, *23*, 2947−2948.

(46) Eswar, N.; Webb, B.; Marti-Renom, M. A.; Madhusudhan, M. S.; Eramian, D.; Shen, M.-Y.; Pieper, U.; Sali, A. Comparative Protein Structure Modeling Using MODELLER. *Curr. Protoc. Protein Sci.* **2007**, 2.9.1.

(47) Webb, B.; Sali, A. Protein Structure Modeling with MODELLER. *Methods Mol. Biol.* **2014**, *1137*, 1−15.

(48) Pettersen, E. F.; Goddard, T. D.; Huang, C. C.; Couch, G. S.; Greenblatt, D. M.; Meng, E. C.; Ferrin, T. E. UCSF Chimera−a Visualization System for Exploratory Research and Analysis. *J. Comput. Chem.* **2004**, *25*, 1605−1612.

(49) Laskowski, R. A.; MacArthur, M. W.; Moss, D. S.; Thornton, J. M. PROCHECK: A Program to Check the Stereochemical Quality of Protein Structures. *J. Appl. Crystallogr.* **1993**, *26*, 283−291.

(50) Chen, V. B.; Arendall, W. B.; Headd, J. J.; Keedy, D. A.; Immormino, R. M.; Kapral, G. J.; Murray, L. W.; Richardson, J. S.; Richardson, D. C. MolProbity: All-Atom Structure Validation for Macromolecular Crystallography. *Acta Crystallogr., Sect. D: Biol. Crystallogr.* **2010**, *66*, 12−21.

(51) Van Durme, J.; Delgado, J.; Stricher, F.; Serrano, L.; Schymkowitz, J.; Rousseau, F. A Graphical Interface for the FoldX Forcefield. *Bioinformatics* **2011**, *27*, 1711−1712.

(52) Labute, P. Protonate3D: Assignment of Ionization States and Hydrogen Coordinates to Macromolecular Structures. *Proteins: Struct., Funct., Genet.* **2009**, *75*, 187−205.

(53) Salomon-Ferrer, R.; Götz, A. W.; Poole, D.; Le Grand, S.; Walker, R. C. Routine Microsecond Molecular Dynamics Simulations with AMBER on GPUs. 2. Explicit Solvent Particle Mesh Ewald. *J. Chem. Theory Comput.* **2013**, *9*, 3878−3888.

(54) Wang, J.; Wolf, R. M.; Caldwell, J. W.; Kollman, P. A.; Case, D. A. Development and Testing of a General Amber Force Field. *J. Comput. Chem.* **2004**, *25*, 1157−1174.

(55) Jakalian, A.; Jack, D. B.; Bayly, C. I. Fast, Efficient Generation of High-Quality Atomic Charges. AM1-BCC Model: II. Parameterization and Validation. *J. Comput. Chem.* **2002**, *23*, 1623−1641.

(56) Lindorff-Larsen, K.; Piana, S.; Palmo, K.; Maragakis, P.; Klepeis, J. L.; Dror, R. O.; Shaw, D. E. Improved Side-Chain Torsion Potentials for the Amber ff99SB Protein Force Field. *Proteins: Struct., Funct., Genet.* **2010**, *78*, 1950−1958.

(57) Jorgensen, W. L.; Chandrasekhar, J.; Madura, J. D.; Impey, R. W.; Klein, M. L. Comparison of Simple Potential Functions for Simulating Liquid Water. *J. Chem. Phys.* **1983**, *79*, 926.

(58) Fuchs, J. E.; Huber, R. G.; von Grafenstein, S.; Wallnoefer, H. G.; Spitzer, G. M.; Fuchs, D.; Liedl, K. R. Dynamic Regulation of Phenylalanine Hydroxylase by Simulated Redox Manipulation. *PLoS One* **2012**, *7*, e53005.

(59) Roe, D. R.; Cheatham, T. E. PTRAJ and CPPTRAJ: Software for Processing and Analysis of Molecular Dynamics Trajectory Data. *J. Chem. Theory Comput.* **2013**, *9*, 3084−3095.

(60) Fuchs, J. E.; Fuchs, D.; Liedl, K. R. Dynamic Regulation of Phenylalanine Hydroxylase. *Pteridines* **2014**, *25*, 33−39.

(61) Huber, R. G.; Eibl, C.; Fuchs, J. E. Intrinsic Flexibility of NLRP Pyrin Domains Is a Key Factor in Their Conformational Dynamics, Fold Stability, and Dimerization. *Protein Sci.* **2015**, *24*, 174−181.

(62) Fuchs, J. E.; Waldner, B. J.; Huber, R. G.; von Grafenstein, S.; Kramer, C.; Liedl, K. R. Independent Metrics for Protein Backbone and Side-Chain Flexibility: Time Scales and Effects of Ligand Binding. *J. Chem. Theory Comput.* **2015**, *11*, 851−860.

(63) van Westen, G. J. P.; Gaulton, A.; Overington, J. P. Chemical, Target, and Bioactive Properties of Allosteric Modulation. *PLoS Comput. Biol.* **2014**, *10*, e1003559.

(64) Ain, Q. U.; Méndez-Lucio, O.; Ciriano, I. C.; Malliavin, T.; van Westen, G. J. P.; Bender, A. Modelling Ligand Selectivity of Serine Proteases Using Integrative Proteochemometric Approaches Improves Model Performance and Allows the Multi-Target Dependent Interpretation of Features. *Integr. Biol.* **2014**, *6*, 1023−1033.

(65) Dunbrack, R. L. Rotamer Libraries in the 21st Century. *Curr. Opin. Struct. Biol.* **2002**, *12*, 431−440.

(66) Hanson, S. M.; Morlock, E. V.; Satyshur, K. A.; Czajkowski, C. Structural Requirements for Eszopiclone and Zolpidem Binding to the Gamma-Aminobutyric Acid Type-A (GABAA) Receptor Are Different. *J. Med. Chem.* **2008**, *51*, 7243−7252.

(67) Buhr, A.; Baur, R.; Malherbe, P.; Sigel, E. Point Mutations of the alpha1betha2gamma2 Gamma-GABAA Receptor Affecting Modulation of the Channel by Ligands of the Benzodiazepine Binding Site. *Mol. Pharmacol.* **1996**, *49*, 1080−1084.

(68) Sigel, E.; Buhr, A. The Benzodiazepine Binding Site of GABA(A) Receptors. *Trends Pharmacol. Sci.* **1997**, *18*, 425−429.

(69) Bergmann, R.; Kongsbak, K.; Sørensen, P. L.; Sander, T.; Balle, T. A Unified Model of the GABA(A) Receptor Comprising Agonist and Benzodiazepine Binding Sites. *PLoS One* **2013**, *8*, e52323.

(70) Renard, S.; Olivier, A.; Granger, P.; Avenet, P.; Graham, D.; Sevrin, M.; George, P.; Besnard, F. Structural Elements of the -Aminobutyric Acid Type A Receptor Conferring Subtype Selectivity for Benzodiazepine Site Ligands. *J. Biol. Chem.* **1999**, *274*, 13370−13374.

(71) Lüscher, B. P.; Baur, R.; Goeldner, M.; Sigel, E. Influence of GABA(A) Receptor α Subunit Isoforms on the Benzodiazepine Binding Site. *PLoS One* **2012**, *7*, e42101.

(72) Wallace, A. C.; Laskowski, R. A.; Thornton, J. M. LIGPLOT: A Program to Generate Schematic Diagrams of Protein-Ligand Interactions. *Protein Eng., Des. Sel.* **1995**, *8*, 127−134.